Heliyon 10 (2024) e31220

Contents lists available at ScienceDirect

Heliyon

journal homepage: www.cell.com/heliyon

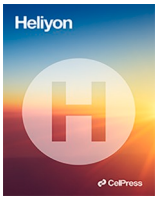

Research article

Agricultural and industrial wastes applied on the high performance energy storage devices

Hsin Her Yu [a,**], Chia-Hua Lin [a], Jau-Jhong Yu [b], Wen-Kai Kuo [b], Hsu-Feng Lee [a,*]

[a] Department of Biotechnology, National Formosa University, 64 Wenhua Road, Huwei, Yunlin, 63208, Taiwan
[b] Graduate Institute of Electro-Optical and Materials Science, National Formosa University, 64 Wenhua Road, Huwei, Yunlin, 63208, Taiwan

ARTICLE INFO

Keywords:
Supercapacitor
Quantum dots
Carbon fiber
Garlic skin
Energy storage device

ABSTRACT

Driven by population growth, the destruction of the environment and the energy demand continue to increase dramatically. This study uses garlic skin and carbon fiber from agricultural and industrial wastes to prepare energy storage devices. Carbon quantum dots (CQDs) were obtained from garlic skin using high-temperature pyrolysis. The specific capacitance of the gel electrolyte could be effectively increased with a small number of CQDs doping. A methylcellulose-based carbon fiber-electrode was prepared by grinding and depositing the industrial recycled carbon fiber onto a biodegradable methylcellulose substrate. The methylcellulose-based recycled carbon fiber-electrode has the highest specific capacitance, energy density, and power density, which are 155 F/g, 10 Wh/kg, and 4047 W/kg, respectively, at a scan rate of 0.02 V/s, and demonstrates excellent performance, such like high specific capacitance, low internal resistance as well as rapid charge and discharge characteristics, which may have potential to replace the expensive carbon nanotubes and graphenes. The electrodes were made from recycled carbon fiber, the gel electrolyte with garlic CQDs, and a separator assembled into a sandwich structure to form supercapacitors. The capacity retention rate of the supercapacitor still retained 96 % of its initial value after 2000 cycles of charge and discharge testing at a constant current of 0.20 mA. This demonstrates the supercapacitor prepared in this study with competitive power density, energy density, high rate capability, and excellent life cycle stability by combining the garlic skin and carbon fiber from agricultural and industrial wastes, highlighting the enormous potential of agricultural and industrial wastes for energy storage applications.

1. Introduction

Energy requirements have shown explosive growth with the economy's growth and society's development in recent years. How to effectively save energy and energy storage has become an important topic in energy science and technology development. Many wearable electronic products have appeared one after another recently to improve people's quality of life greatly. However, no matter what kind of electronics are used, a continuous energy supply is required to function smoothly. This also shows that developing efficient energy storage devices is crucial. As the global population increases yearly, so does the demand for food and industrial products. Meanwhile, developing alternative sustainable energy sources and searching for raw material supplies are required. The

* Corresponding author.
** Corresponding author.
E-mail address: hhyu@nfu.edu.tw (H.-F. Lee).

https://doi.org/10.1016/j.heliyon.2024.e31220
Received 25 January 2024; Received in revised form 24 April 2024; Accepted 13 May 2024
Available online 14 May 2024

global annual generation of biomass waste is in the order of 140 Gt [1]. In the case of agricultural products, inedible parts, such as oyster shells, corn stalks, and garlic skins, are often discarded arbitrarily or burned in the open. In addition, in the case of industrial products, there are also many leftovers, such as chips after metal cutting, cotton wool leftovers after making towels, and carbon fiber leftovers after making blades for drones or wind turbines, resulting in significant environmental impacts.

The awareness of people's environmental responsibility has gradually increased after the signing and initiating of the Paris Agreement and the Kyoto Protocol [2,3]. Problems arising from manufacturing and the environment are gradually attracted since many agricultural or industrial wastes cannot be decomposed naturally. Generally, biochar is highly stable and comprises more than 65 % carbon [4]. The biochar can be produced from various feedstocks (forestry, agricultural, aquatic biomasses, livestock detritus, industrial and municipal wastes) by various common production techniques, such as pyrolysis, gasification, carbonization, hydrothermal carbonization as well as torrefaction [5]. This study applies the concept of environmental waste reduction from the viewpoint of circular economy. Carbon quantum dots (CQDs) and the electrodes are prepared from the garlic skins and the recycled carbon fibers (C-fibers). Then, both are applied to assemble the energy storage devices simultaneously. From a circular economy perspective, this study uses environmental waste reduction and then applies it to producing energy storage devices [6]. Owing semiconductor or metal quantum dots (QDs) do not dissolve each other in aqueous solutions; they must be coated with hydrophilic molecules before they can be used in biological areas [7]. However, this undoubtedly increases the energy cost of the QD production process and produces more waste. CQDs prepared from plants have the advantage of high biocompatibility [8,9]. Additionally, the hydrophilic properties of the surface still exist even if prepared by hydrothermal synthesis [10,11]. These hydrophilic functional groups can maintain good dispersion characteristics of CQDs in water, and if they are used, they will have good application prospects.

In response to greenhouse gas emission reduction and removal, there has been a lot of research on using plants as green carbon sources. For example, starch extracted from corn stalks and other plants can be used as raw materials for CQDs [12]. Rice, coconut, and other seed husks have also been widely investigated [13]. Many researchers even synthesize CQDs from charcoal made from various plants [14]. There are many methods for preparing CQDs, but high-pressure hydrothermal synthesis is the most common technique [15]. The carbon source is sealed in a container filled with pure water or other aqueous solutions and heated at a temperature between 150 and 260 °C for several hours to decompose. This simple fabrication process makes it easy to produce CQDs. In addition, CQDs can also be prepared by laser processing technology [16] or microwave plasma treatment technology [17].

C-fibers are widely applied in aeronautical engineering, automobile manufacturing, biotechnology, and medical fields since they have the advantages of high elastic modulus, high mechanical strength, and chemical corrosion resistance. Since composites have different application requirements, C-fibers are often pre-treated before being prepared into composites to achieve the appropriate interfacial bond strength. C-fibers are usually modified by changing their surface morphology or introducing chemical agents to improve the adhesion between fiber stacks by thermal treatment, plasma treatment, chemical vapor deposition, and chemical grafting in recent years [18]. However, the application of the waste C-fibers generated in the production process has not been effectively proposed. If the current situation of direct disposal of these wastes can be improved, it will undoubtedly indicate corporate responsibility and waste reduction.

On the other hand, there are many CQDs prepared from agricultural wastes. Still, only a few studies have originated from garlic skins, and their main use is in applying fluorescent sensors [19]. However, CQDs were synthesized from garlic skins using high-temperature pyrolysis technology rather than the high-pressure hydrothermal method in this study.

In this study, CQDs were obtained from garlic skins by high-temperature pyrolysis method and added with PVA and H_3PO_4 to produce a gel-electrolyte, and cyclic voltammetry and AC impedance analysis was performed by multifunctional cyclic voltammetry. The carbon fiber suspension was made by grinding the recycled C-fiber and dispersing it in Arabic gum, then depositing it on the methylcellulose substrate to obtain the carbon fiber-based electrodes. Cyclic voltammetry and internal resistance analysis were carried out. In addition, a supercapacitor was assembled with carbon fiber-based electrodes, CQDs doping gel electrolytes, and a separator in a sandwich configuration. The multi-function cyclic voltammetry analyzer performs cyclic charge and discharge tests to understand the capacitance maintenance rate of supercapacitors. Two types of waste were recycled and reused in the energy area in this study. From the perspective of the UN's sustainable development goals (SDGs), it is helpful for climate change mitigation and adaptation. Solving energy problems without forgetting environmental responsibility will be a sustainable trend and long-term goal in the future.

2. Experimental

2.1. Preparation of carbon quantum dots doped gel electrolyte

The waste garlic skins were chopped to shorten the fiber length and then carbonized at 240 °C for 2 h to form the CQDs precursor. The CQDs precursor was immersed in a mixture of disodium hydrogen phosphate, sodium hydroxide, and deionized water. Subsequently, the solution was centrifuged at 9000 rpm for 30 min, and the supernatant was collected and filtered through filter paper again. The filtered filtrate was ultrasonically dispersed in an ultrasonicator at 900 Hz for 2 h, and then the supernatant was sealed and protected from light for 24 h and dialyzed for 12 h. Finally, the CQDs were obtained after freeze-drying at −80 °C overnight. A uniformly dispersed CQD suspension was prepared to fabricate the electrodes by mixing CQDs with deionized water at a 1 mg/ml ratio prior to use.

PVA aqueous solution was prepared by dissolving 10 g of polyvinyl alcohol (PVA, Mw 85,000–120,000 g/mol, Sigma) in 100 ml of deionized water at 85 °C. Subsequently, H_3PO_4 was added dropwise into the stirred PVA solution to obtain a homogenous PVA/H_3PO_4 solution. Then, the aqueous solution was dried in a vacuum oven at 60 °C for 6 h to form the PVA/H_3PO_4 gel electrolyte. To evaluate the effect of adding CQDs on the electrochemical performance to gel electrolyte, different proportions (0.05, 0.10, 0.15, 0.20 %) of

CQDs suspension were added into the PVA/H_3PO_4 gel electrolyte.

2.2. Preparation of carbon fiber-based electrodes and supercapacitors assembling

Long strips of carbon fiber waste were shredded to shorter fiber lengths, and then C-fibers were cleaned with a neutral detergent to remove excess impurities. The C-fibers were ground with 20 ml alcohol in the mortar for 1 h, then ground in a planetary ball mill for 24 h in a ratio of 1:10 (carbon fiber to alcohol) by mass. The fine C-fibers were then centrifuged at 4000 rpm for 20 min, and the precipitates were dried in a vacuum oven overnight to obtain the fine C-fiber powders before use.

The methyl-cellulose (4 g, purchased from Sigma) was added to 100 ml of ethyl alcohol and stirred at 60 °C until the powders dissolved completely. The methylcellulose substrates were obtained by casting the alcohol solutions of the methylcellulose onto a flat glass plate, drying at room temperature under vacuum for 15 min, and then at 50 °C for an additional 2 h.

The carbon fiber suspension was prepared using Arabic gum to disperse the fine carbon fiber powder in deionized water. Briefly, 0.5 g of fine C-fiber powder was added into 0.5 wt% of Arabic gum aqueous solution with magnetic stirring for 1 h, followed by ultrasonication for 4 h. Subsequently, the C-fiber suspension was centrifuged twice at 6000 rpm for 25 min in a high-speed centrifuge, and the supernatant was retained to obtain a uniformly dispersed C-fiber conductive suspension. To fabricate the electrode, 2 ml of C-fiber conductive suspension was dropped onto the methylcellulose substrates and dried at 50 °C overnight to obtain the methylcellulose-based C-fiber electrode.

The supercapacitors were assembled from two C-fiber coated, methylcellulose-based electrodes and a nylon mesh as separator enclosed with the CQDs-containing PVA/H_3PO_4 gel electrolyte.

2.3. Characterization

2.3.1. Carbon quantum dots analysis

The TGA instrument analyzed the thermal stability of garlic skin and carbon fiber (Mettler-Toledo, 2-HT). The average particle size and surface potential of the CQDs from carbonized garlic skin were analyzed by a zeta potential analyzer (Zetasizer; 3000HS, Malvern Instruments). The surface morphology of CQDs was investigated by field emission scanning electron microscopy (FESEM, JSM-6700F, JEOL) and penetrating electron microscopy (PHILIPS CM-200, TEM). Subsequently, The UV–Vis spectroscopy of the diluted 1000 times carbon quantum dots conductive liquid was recorded using an ultraviolet–visible spectrometer (Jasco V-730). In addition, to determine the possible functional groups on the surface of the prepared CQDs, the FTIR spectroscopy of the CQDs coated on the CaF_2 was recorded by using ThermoFisher Scientific Inc. Nicolet iS5 spectrometer at a resolution of 4 cm^{-1} from 4000 to 400 cm^{-1}. The X-ray photoelectron spectrometer facility (XPS; JEOL JAMP-9500F) experiments were carried out at room temperature to confirm C-fiber characteristics in an ultrahigh-vacuum (UHV) system with the surface analysis system.

2.3.2. Analysis of gel electrolyte electrochemical characteristics

Electrochemical measurements were performed in a three-electrode electrochemical cell to investigate the electrochemical properties of the methylcellulose-based C-fiber electrodes and supercapacitors. All electrochemical characteristics were evaluated by cyclic voltammetry (CV), and the galvanostatic charge/discharge and cycle life measurements were recorded on a CHI627E electrochemical workstation (CH Instruments, Inc.) Using a three-electrode cell consisting of the methylcellulose-based C-fiber electrodes as the working electrode, Pt wire, and Ag/AgCl as the counter and reference electrodes, respectively, and 1 M H_3PO_4 as the electrolyte. CV measurements were carried out in the potential range of 0.0–0.7 V at scan rates of 0.02–0.20 V/s.

In the three-electrode cell, the specific capacitance (Cs, F/g) of the porous and sandpaper-based electrodes was calculated according to Eq. (1) [20], i.e., the specific capacitance of the electrode is equal to the cell capacitance divided by the weight of the active material in the working electrode:

$$Cs = \frac{\int i dV}{m * s * \Delta V} \tag{1}$$

where i (mA) is the discharge current, m (g) is the weight of the active material, s (V/s) is the scan rate, ΔV (V) represents the operating potential window. In addition, the energy density (ED, Wh/kg) and power density (PD, W/kg) of the methylcellulose-based carbon fiber electrodes can be calculated according to Eqs. (2) and (3) [21], respectively:

$$ED = \frac{1}{2}\frac{1000}{3600} Cs * V^2 \tag{2}$$

$$PD = \frac{ED * 3600}{t} \tag{3}$$

where t (s) is the discharge time during the scanning period.

Electrochemical impedance spectroscopy (EIS) measurements were carried out with a chemical impedance analyzer from 100 kHz to 0.01 Hz. The capacitance behavior and cycle stability of the sandwiched supercapacitors were also investigated at a consistent current of 0.20 mA.

3. Results and discussion

3.1. Thermogravimetric analysis of garlic skin and carbon fiber

The thermal stability of the garlic skin and carbon fiber was measured using TGA analysis from room temperature to 600 °C. The results are shown in Fig. 1. The TGA of carbon fiber showed almost no loss, and the residual weight was 97.82 % at 600 °C. The TGA of garlic skin exhibited three major steps of thermal degradation. Initially, the weight loss was around 50–140 °C due to the removal of water in the garlic skin. Jeevan determined the residual char of garlic skin is 35 % at 600 °C by TGA [22]. The residual weight of garlic skin was 24.5 % at 600 °C in this study; considering the 8 % loss from water, the real residual weight is 32.5 %; this is agreed with the published reference. Furthermore, the garlic skin was converted to CQD precursor at 240 °C for 2 h, and the residual weight of CQD precursor remained over 80 %, according to Fig. 1; this confirmed that the conversion rate is successfully high and can provide enough carbon content as CQDs for the energy storage device.

3.2. Surface analysis results of carbon quantum dots

CQDs generally are typical zero-dimensional quasi-spherical shaped nanoparticles with less than 10 nm particle size and exhibiting a quantum confinement effect. Surface potential is an important parameter for studying the interaction between two surfaces. Adsorption is one kind of interaction between adsorbate and adsorbent. Here, the average particle size of the papered garlic CQDs was 7 nm through particle size analysis and potential analysis. The measured size distribution histogram is shown in Fig. 2(a). The particle size of obtained CQDs in this study is similar to the reported reference published by Tong [23]. The garlic CQDs surface potential was examined by zeta potential measurement in Fig. 2(b). The obtained zeta potential is +0.00364 mV. The absolute zeta-potential values above |±30 mV| were considered moderately stable against aggregation due to charge stabilization [24]. Therefore, adding a very small amount of garlic CQDs to the electrolyte can help improve the electrical properties. Bui reported the CQDs by one-pot hydrothermal method directly from lemon juice at different temperatures. The CQDs synthesized at 200 °C and 240 °C exhibit distinguish size distribution in the ~12–15 nm range and 3–5 nm, respectively. The prepared CQDs show around 50 nm agglomeration particle size under DLS measurement and a 9.48 mV zeta potential value [25]. Fig. 2(c) and (d) show the SEM and TEM images of the garlic CQDs, respectively. The surface morphology shows the formation of spherical-like carbon particles after the carbonization process. The size of the spherical CQDs is about 250 nm, as shown in Fig. 2(c). The aggregated spheres were diluted 1000 times, and it was found that the CQDs could be dispersed well in water without accumulation. The size of prepared CQDs is confirmed to be about 6–10 nm, determined by TEM, as shown in Fig. 2(d). Tong [23] has extracted CQDs from empty fruit bunch (EFB) biochar using a green acid-free microwave method and reported a similar spherical form with 2.6 ± 0.6 nm particle size. Canan [26] prepared the CQDs with nitrogen-containing nitrogen using the green synthesis method from the *Kombucha fungus* and confirmed the particle size to be 5 nm. Furthermore, The CQDs were used as electrode materials for supercapacitors and demonstrated an improved charge-discharge cycle. In this study, a small amount of CQDs is added to the electrolyte and expected to increase the specific capacitance value of the electrolyte without agglomeration.

3.3. UV-VIS and FTIR analysis of garlic carbon quantum dots

Fig. 2(e) shows the UV/VIS spectrum of a diluted 1000 times carbon quantum dot solution. The absorption peak of the prepared sample in the UV/VIS region is related to the absorption of CQDs, and a typical electronic transition n-π* transition peak is observed at

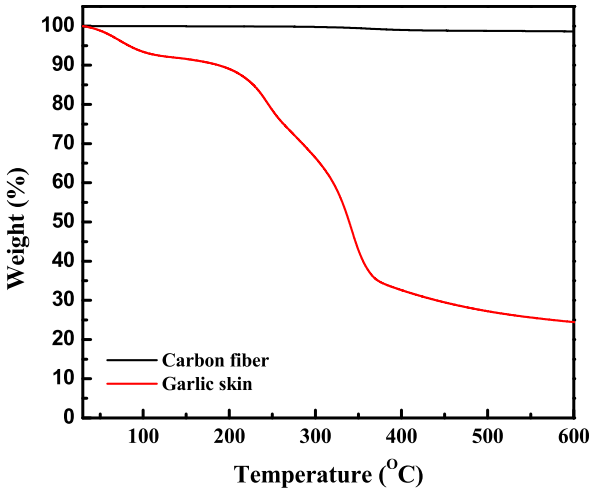

Fig. 1. The TGA graph of garlic skin and Carbon fiber.

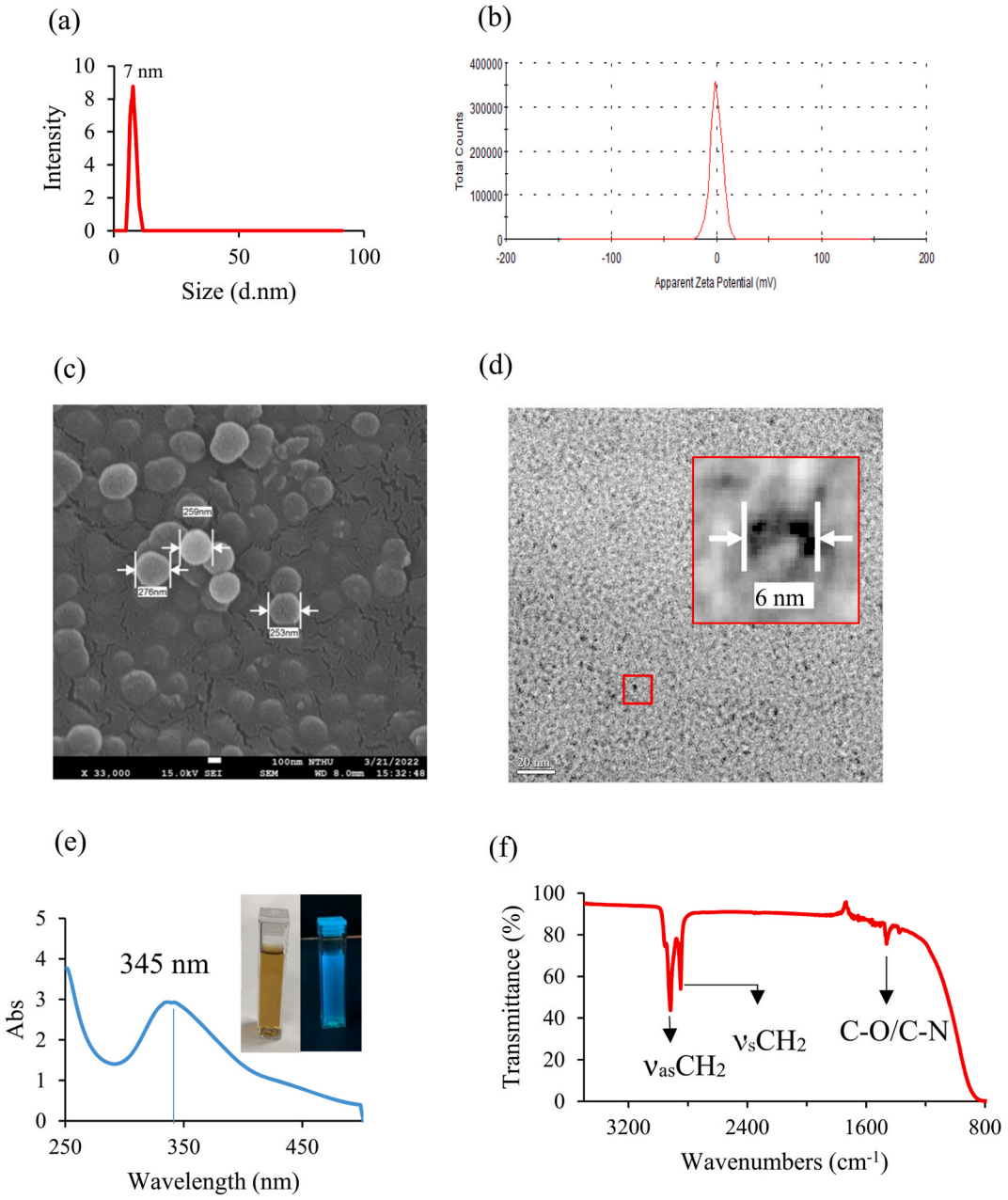

Fig. 2. The carbon quantum dots from garlic skin: (a)Particle size analysis; (b)Surface zero potential analysis; (c)SEM image; (d) TEM image; (e) UV–Vis spectrum of CQDs, brown color of CQDs aqueous solution under sunlight (left insert) and UV light irradiation (right insert); (f) FTIR spectrum of garlic peel CQDs. (For interpretation of the references to color in this figure legend, the reader is referred to the Web version of this article.)

345 nm due to the presence of oxygen-containing functional groups (such as C–O, C═O) at the surface of CQDs [27]. The inset graphs in Fig. 2(f) show the aqueous CQDs solution under sunlight and UV–Vis irradiation. The color of the former under sunlight is yellow-brown, and the latter is blue due to the CQDs being excited to emit the fluorescence under ultraviolet irradiation.

The FTIR spectrum of the CQDs is provided to confirm the functional groups of CQDs, as shown in Fig. 2(f). An absorption position at around 1463 cm^{-1} refers to the C–O/C–N bending vibration mode; this confirmed that the surface of CQD prepared from garlic skin contains an oxygen/nitrogen functional group [28,29]. In addition, the two absorption peaks that appeared at 2918 and 2848 cm^{-1} corresponded to CH_2 asymmetric and symmetric stretching modes [30], respectively. XPS will carry out further investigation and explain.

3.4. XPS analysis of garlic carbon quantum dots

To further confirm the functional groups on the surface of the carbonization garlic, the prepared CQDs sample was analyzed by XPS in this study. Fig. 3(a) shows the XPS spectrum at around 284.8, 400.8, and 532.8 eV, representing C1s, N1s, and O1s, respectively, which correspond to the atomic ratio of C/N/O s is 60.9, 28.4 and 10.7 %. The C1s spectrum of CQDs can be deconvoluted into four contributions at 285 eV (C–H), 288.3 eV (C═O), 286.7 eV (C–*O*–C), and 289.3 eV (O–C═O), as shown in Fig. 3(b). The N1s peak at 399.8 eV, 399.9 eV, and 400.3 eV corresponded to N-(C═O), N-(C═O)–N, and N-(C═O)–O functional groups, respectively, as shown in Fig. 3(c). In addition, the peak at 399.7 eV is likely to be related to the amide bond, which also corresponds to the N–H bending vibration in the FTIR spectrum. The O1s peaks at 531.8 eV can be assigned to the C═O bond, as shown in Fig. 3(d), and no other oxygen peaks are observed. This suggests that the prepared CQDs in this study have no carboxylic acid functional group but contain carbonyl and amide functional groups.

3.5. Effect of adding garlic carbon quantum dots on the specific capacitance of gel electrolyte

Fig. 4(a) represents the CV curves of CQD-adding into H_3PO_4/PVA gel electrolyte with different percentages. The CV curves area are 4.84×10^{-6}, 1.15×10^{-5}, 1.24×10^{-5}, 1.10×10^{-5}, and 1.08×10^{-5} cm^2 when the CQDs adding ratio are 0, 0.05, 0.10, 0.15–0.20 % to the electrolyte, respectively. This implies the CV areas increase first and then decrease with increasing the content of CQDs. In addition, the specific capacitance of the 1 M H_3PO_4/PVA gel electrolyte with different ratios of added CQDs could be calculated by Eq. (1), and the results are presented in Fig. 4(b). The 1 M H_3PO_4/PVA gel electrolyte with 0, 0.05, 0.10, 0.15, and 0.20 % addition have the specific capacitances of 0.002, 51.53, 110.57, 32.57, and 23.98 F/g at scanning rate of 0.02 V/s, respectively. Noteworthy, the specific capacitance of 1 M H_3PO_4/PVA gel electrolyte with 0.1 % CQD adding exhibits the highest value in these study cases, possibly due to a small doping of CQDs increase the charge transfer capacity of the electrolyte resulting in the lower internal resistance, hence increases the specific capacitance. In the earlier discussion, the prepared CQDs are determined to cause nanoparticle aggregation due to the lower zeta potential value. The specific capacitance decreased to 23.98 F/g when 0.20 % of the CQDs were added to 1 M H_3PO_4/PVA gel electrolyte, which may be attributed to the agglomeration of excess CQDs in the gel electrolyte, resulting in a decrease in the poor charge transfer efficiency between ions, hence lower the in the specific capacitance. In summary, we concluded that the small addition of trace amounts of CQDs can significantly improve the specific capacitance of the electrolyte, which is benefit to the supercapacitors.

3.6. Effect of adding carbon quantum dots on the equivalent series resistance of gel electrolyte

In this study, the electrochemical impedance spectroscopy (EIS) measurement is an important characterization tool used to evaluate the resistive behavior of adding carbon quantum dots to the electrolyte. Fig. 4(c) shows the respective Nyquist plots for the addition of carbon quantum dots with a different percentage in the gel electrolyte between 100 and 1 M Hz, where Z' (X-axis) is the real

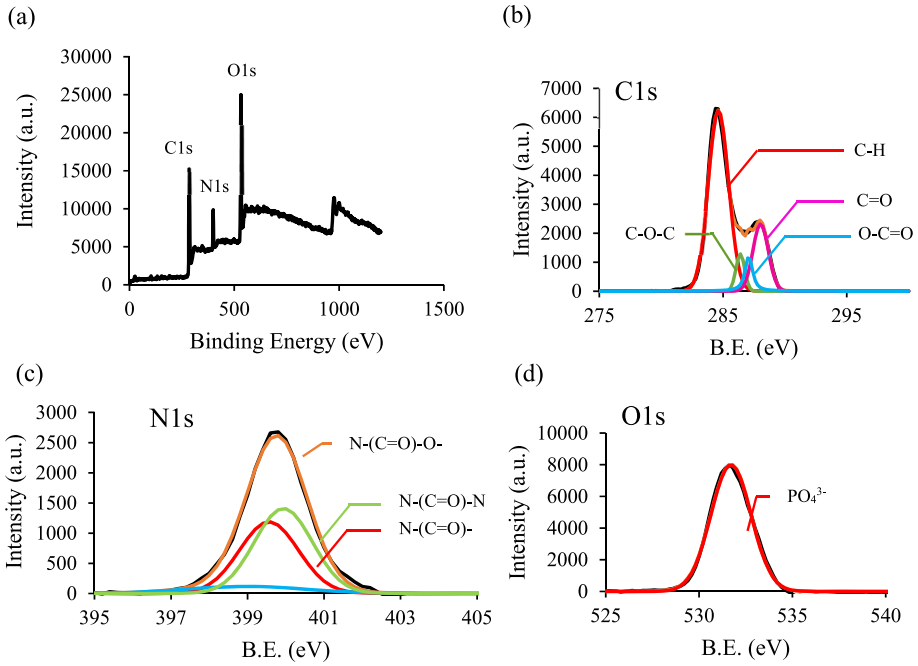

Fig. 3. (a) Completely measured high-resolution XPS spectrum of garlic peel CQDs; XPS spectra of (b) C1s; (c) N1s; (d) O1s.

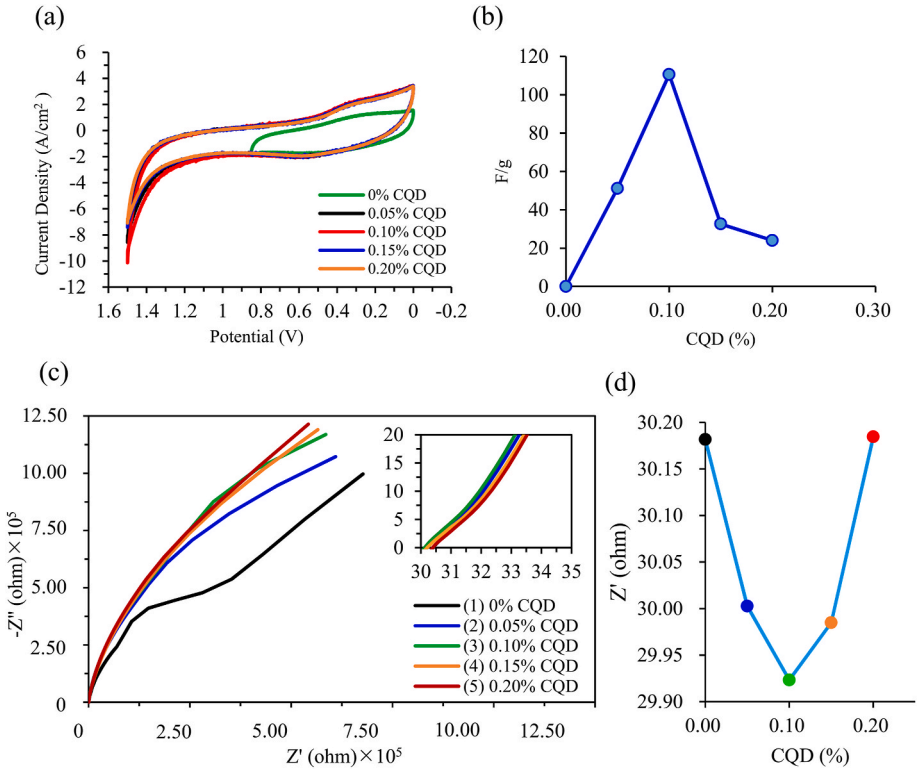

Fig. 4. (a) Cyclic voltammetry curves; (b) specific capacitance values of different concentrations of CQDs adding to the phosphoric acid gel electrolyte; (c) AC impedance analysis curves at (i) low frequency region, (ii) high frequency region; (d) ESR change for different concentrations of CQDs adding to phosphoric acid gel electrolyte.

part and Z'' (Y-axis) is the imaginary part of the impedance. Fig. 4(c) and insert graph represent the high-frequency region vs. low-frequency region in the AC impedance. The Nyquist plots of all samples consist of a semicircle in the high-frequency region and an inclined line along the imaginary axis with an angle of 45° in the low-frequency region. The size of the cole-cole plot semicircle in the high-frequency region generally reflects the charge transfer process. The product or reactant of the electrode reaction reflects the diffusion impedance curve in the low-frequency region [31].

The line feature of an ideal capacitor is the curve in the low-frequency region is perpendicular to the Z′ axis and close to the Z″ axis, indicating that the diffusion resistance is smaller and allows ions to transfer between the electrode surface [32]. Fig. 4(c) represents the EIS curves of all electrolytes with and without adding quantum dots in the low-frequency region. The electrolyte with 0 % CQDs addition shows a Warburg region with a 45° angle in the low-frequency region related to the ionic diffusion between electrolyte and electrode. This indicates the high diffusivity resistance. The insert graph in Fig. 4(c) shows EIS curves of the addition of different CQDs in the gel electrolyte in the high-frequency region. The equivalent series resistance (ESR) values of gel electrolytes are 30.18, 30.00, 29.92, 29.98, and 30.18 Ω when CQDs are added into electrolytes with 0, 0.05, 0.10, 0.15, and 0.20 %, respectively, as shown in Fig. 4 (d). Notably, the lowest ESR value is found in this study when doping with 0.10 % of CQDs into electrolytes. This also can explain the earlier CV results and why the highest specific capacitance is determined in Fig. 4(b). However, the ESR values decreased when the excess amounts of carbon quantum dots were added from 0.10 to 0.20 %, decreasing specific capacitance, as shown in Fig. 4(d). Cheng [33] reported a novel nanocomposite polymer electrolyte by introducing the CQDs with 2–3 nm nanofiller into a poly (ethylene oxide) (PEO) matrix. The PEO/CQDs-Na nanocomposite polymer electrolyte exhibits an exceptionally high ionic conductivity due to the homogeneous dispersion of CQDs at 3 wt% within the PEO matrix. Furthermore, the inserted graph in Fig. 4(c) shows almost no semicircle curve formation, which implies that the charge transfer resistance in the electrolyte is extremely small, resulting in a good charge transfer efficiency between the electrolyte and electrode surface.

3.7. Cyclic voltammetry analysis of methylcellulose-based carbon fiber electrodes

In a three-electrode electrochemical cell, the ideal cyclic voltammetry curve should appear in a shape close to rectangular. However, a contact resistance or internal resistance of the electrolyte will occur due to the contact between the electrode and the electrolyte, resulting in an ideal cyclic voltammetry curve swift from the ideal shape [34]. Fig. 5(a) shows the cyclic voltammetry curve of a methylcellulose-based C-fibers electrode tested in phosphoric acid at a scanning rate of 0.20 to 0.02 V/s. All curves exhibit symmetrical shapes at different scanning rates, which shows that the electrode has superior capacitance properties and ideal redox

characteristics. The specific capacitance of the methylcellulose-based C-fibers electrode at a scanning rate of 0.20 to 0.02 V/s can be calculated according to eq (1). The results are presented in Fig. 5(a) and listed in Table 1. The specific capacitance of methylcellulose-based carbon fiber electrode increased with decreasing the scan voltage, and at 0.02, 0.10, 0.05, and 0.02 V/s are 46.68, 76.10, 107.9, and 155.58 F/g, respectively. It is obvious that the specific capacitance of the methylcellulose-based C-fibers electrode at 0.02 V/s has the highest value among all scan rates. This might be attributed to the high surface area of the C-fiber electrode, which allowed more ions to charge onto the carbon fiber electrode at a lower scan rate, similar to our previous results [35]. In addition, the energy density (ED) and power density (PD) of the methylcellulose-based carbon fiber electrode at different specific capacitances can also be calculated by eqs. (2) and (3). the energy density (ED) and power density (PD) of the methylcellulose-based carbon fiber electrode were 4.18, 5,18, 7,34, and 10.59 Wh/kg and 1214, 1979, 2806, 4047 W/kg at the specific capacitance of 46.68, 76.10, 107.9 and 155.58 F/g, respectively, as listed in Table 1. The specific capacitance values of other electrodes prepared by other researchers were also compared in this study. The scan rate, voltage range, and their specific capacitance are listed in Table 2. The electrode prepared in this study using recycled C-fibers has the highest specific capacitance value of 155.58 F/g compared to CNT, rGO, and MWCNT-based electrodes [36–38]. Furthermore, the methylcellulose-based C-fiber electrode demonstrates excellent performance than other reported modified activated carbons [39], carbon nanotubes [40–42] as well as graphenes [43–48], as shown in Fig. 6(a). It also displays that C-fiber has a high potential to replace the expensive carbon nanotubes and graphenes.

The ratio of the absolute difference between capacitance values measured at two scan rates and the capacitance at the higher scan rate is known as the attenuation rate (α, %). As the attenuation rate increases, the rate capability (β) decreases. The rate capability of the capacitance can be obtained as follows [49]:

$$\Delta Cs = |Cs_l - Cs_h| \tag{4}$$

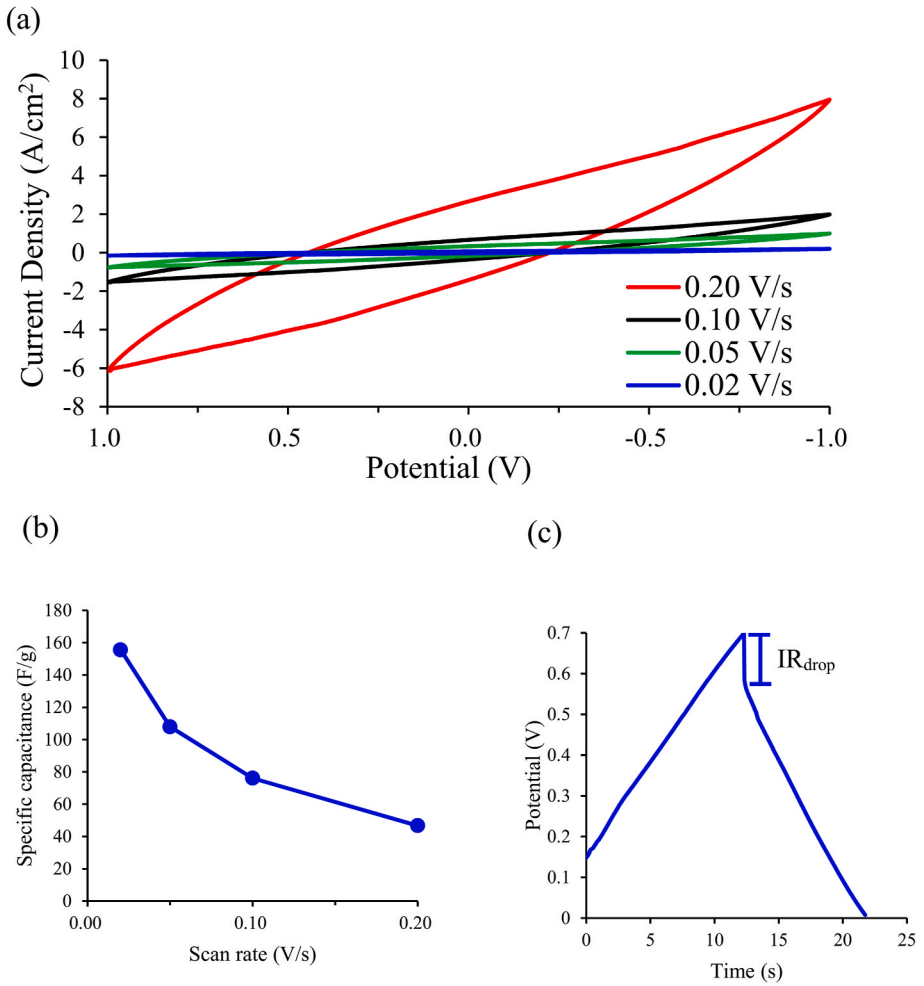

Fig. 5. The methyl cellulose-based recycle-carbon fiber electrode in phosphoric acid electrolyte (a) Cyclic voltammetry curves under different scan rates; (b)Specific capacitance at different scan rates; (c) The galvanostatic charge/discharge graph and internal resistances at a constant current of 0.20 mA.

Table 1
Specific capacitance values of methylcellulose-based carbon fiber electrodes at different scan rates.

Scan rate (V/s)	Electrolytes	Specific capacitance (F/g)	Energy density (Wh/kg)	Power density (W/kg)
0.20	PVA/H_3PO_4	46.68	3.18	1214
0.10	PVA/H_3PO_4	76.10	5.18	1979
0.05	PVA/H_3PO_4	107.90	7.34	2806
0.02	PVA/H_3PO_4	155.58	10.59	4047

Table 2
Comparison of specific capacitance values of different electrodes.

Substrates	Electrode materials	Gel Electrolytes	Scan rate (V/s)	Voltage range (V)	Specific capacitance (F/g)	Ref.
MXene Fiber	Mxene/CNTs	PVA/H_2SO_4	0.20	−0.6–0.3	142.10	[36]
Carbon Cloth	PEDOT:PSS-rGO	PVA/H_3PO_4	0.10	0–1.0	73	[37]
Sandpaper	G/MWCNTs	PVA/H_3PO_4	0.02	0–0.7	55	[38]
Methylcellulose	Recycle C-fiber	PVA/H_3PO_4	0.02	0–0.7	155.58	Our work

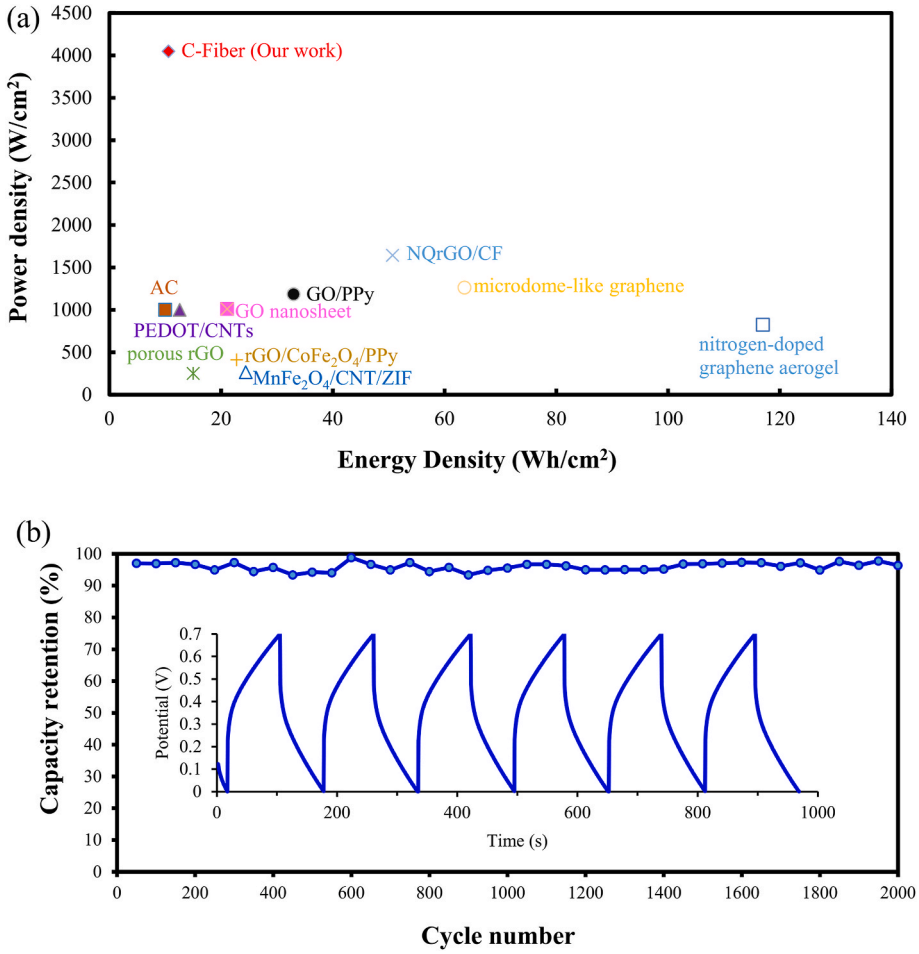

Fig. 6. (a)The performance comparison of the C-Fiber based electrode verses literature reported values of modified carbon sheets, activated carbons, carbon nanotubes, graphenes. (b)The results of the electrode of methyl cellulose-based recycle-carbon fiber after 2000 cycles of charge-discharge tests at a constant current of 0.20 mA.

$$\alpha = \frac{\Delta Cs}{Cs_h} \times 100\% \tag{5}$$

$$\beta = 1 - \alpha \tag{6}$$

where the Cs_h and Cs_l are the specific capacitance values at high and low scan rates; ΔCs (F/g) is the absolute value of the difference in capacitance between two scan rates. The β value for the methylcellulose-based carbon fiber electrode is 70.32 %, according to Eq. (6) and Fig. 5(b). The β value methylcellulose-based C-fiber electrode is lower than our previous results; this suggested that more ions adsorb on the electrode and enhance the energy storage rate for the EDLC at a low scan rate [35,38], which caused the higher decay rate, therefore, lower the β value. Fig. 5(c) presents the galvanostatic charge/discharge testing results of the methylcellulose-based carbon fiber electrode at a current of 0.20 mA. The ideal constant-current charge and discharge pattern is an isosceles triangle shape. However, the impedance occurs when the charge ions are released from the electrodes and return to the electrolyte during discharge. This impedance is called the internal resistance (iR_{drop}). Decreasing the iR_{drop} value can avoid unnecessary energy consumption and waste heat generation during the discharge process and increase specific capacitance [50,51]. The iR_{drop} value of the methylcellulose-based carbon fiber electrode is 0.122 V, significantly smaller than the sandpaper-based electrode (0.161V) in our previous study. As a result, the curve of charge and discharge process of the carbon fiber electrode prepared in this study demonstrated in the shape of an isosceles triangle, which confirmed that the methylcellulose-based C-fibers electrode exhibits excellent rapid charge and discharge characteristics and good reversibility.

3.8. Electrochemical analysis of supercapacitors

Garlic skin and carbon fiber from agricultural and industrial wastes are used to prepare energy storage devices. Fig. 6(b) shows the galvanostatic charge/discharge curve of a sandwiched structure supercapacitor obtained at a current of 0.20 mA over about 2000 cycles in which 0.1 % CQD is added to the gel electrolyte and used a filter paper as separator. The capacitance retention rate of carbon fiber electrode-based supercapacitor remains at 96 % of the initial capacitance. The supercapacitor prepared with carbon fiber electrode and 0.1 % CQD added gel electrolyte exhibits capacitance retention of 96 %, representing excellent cyclic stability in comparison with reported bio-mass derived carbon such as potato starch-based activated carbon shows 86 % capacitance retention over 900 cycles [52], and CQDs-incorporated with ferrous-coordinated polypyrrole (CQDs/PPy-Fe) as electrode of supercapacitor shows of 94.6 % after 2000 cycles [53], as well as *Cassia Fistula* dry fruits biomass converted activated carbon as electrodes for supercapacitor maintained ~86 % of its initial capacitance after 2000 cycles [54]. The result confirmed that the high capacitance retention rate of carbon fiber electrodes indicates their good electrochemical behavior and cycling stability. This may contribute to the appropriate amount of CQDs in the electrolyte, reduce the internal resistance, and increase the charge transfer efficiency when introducing the carbon fiber electrode. This study suggests that the prepared CQDs from the agricultural garlic skin and electrodes from industrial waste C-fibers might have potential in future applications on flexible and wearable electronic devices and energy storage devices.

4. Conclusions

This study successfully prepared CQDs and conductive electrodes from garlic skin and recycled C-fibers using high-temperature pyrolysis and grinding methods. The specific capacitance can reach 110.57 F/g, and the equivalent series resistance can be effectively reduced to 29.92 Ω as 0.10 % CQDs are added into the gel electrolyte. In addition, the specific capacitance value, energy density, and power density of carbon fiber-based electrodes can reach 155 F/g, 10 Wh/kg, and 4047 W/kg at a scan rate of 0.02 V/s, respectively. The supercapacitor with sandwiched structures retains its initial value of 96 % after 2000 cycles of charge and discharge tests under a constant current test of 0.20 mA. This research verified using environmental factors such as agricultural and industrial wastes to manufacture energy storage devices. From the circular economy perspective, it is consistent with the goal of sustainable environmental development of the United Nations SDGs.

Data availability statement

Most of the data are available in all the tables and figures in the manuscripts. Moreover, the data will be available on request.

CRediT authorship contribution statement

Hsin Her Yu: Supervision, Resources, Investigation, Conceptualization. **Chia-Hua Lin:** Methodology, Formal analysis. **Jau-Jhong Yu:** Visualization, Investigation, Data curation. **Wen-Kai Kuo:** Methodology, Formal analysis. **Hsu-Feng Lee:** Writing – review & editing, Writing – original draft, Visualization, Methodology, Formal analysis.

Declaration of competing interest

The authors declare the following financial interests/personal relationships which may be considered as potential competing interests:Hsin Her Yu reports financial support was provided by National Science and Technology Council TW. Hsin Her Yu has patent pending to National Formosa University.

Acknowledgments

The authors gratefully acknowledge the financial support from the National Science and Technology Council (NSTC 111-2221-E-150-006-MY3). The authors also thank Miss Ting-Yin Cheng, who was in service at the instrumentation center of National Tsing Hua University for the Thermogravimetric analysis (TGA).

References

[1] N. Tripathi, C.D. Hills, R.S. Singh, Biomass waste utilisation in low-carbon products: harnessing a major potential resource, npj Clim. Atmos. Sci. 2 (2019) 35, https://doi.org/10.1038/s41612-019-0093-5.
[2] X. Huang, I. Kainat, M. Hasan, Investigation of pretreatment parameters for bioethanol production from Spirogyra using ZnO nanoparticles, Biomass Conv. Bioref. (2023), https://doi.org/10.1007/s13399-023-05024-9.
[3] G. Tatrari, M. Karakoti, C. Tewari, S. Pandey, B.S. Bohra, A. Dandapat, N.G. Sahoo, Solid waste-derived carbon nanomaterials for supercapacitor applications: a recent overview, Mater. Adv. 2 (2021) 1454–1484, https://doi.org/10.1039/D0MA00871K.
[4] S. Wijitkosum, P. Jiwnok, Elemental composition of biochar obtained from agricultural waste for soil amendment and carbon sequestration, Appl. Sci. 9 (2019) 3980, https://doi.org/10.3390/app9193980.
[5] B. Khiari, M. Jeguirim, L. Limousy, S. Bennici, Biomass derived chars for energy applications, Renew. Sustain. Energy Rev. 108 (2019) 253–273, https://doi.org/10.1016/j.rser.2019.03.057.
[6] A. Boruah, M. Saikia, T. Das, R.L. Goswamee, B.K. Saikia, Blue-emitting fluorescent carbon quantum dots from waste biomass sources and their application in fluoride ion detection in water, J. Photochem. Photobiol. B Biol. 209 (2020) 111940, https://doi.org/10.1016/j.jphotobiol.2020.111940.
[7] L. Bar, F. Perissinotto, L.R. Morata, M.I. Giannotti, J. Goole, P.L. Pérez, Interactions of hydrophilic quantum dots with defect-free and defect containing supported lipid membranes, Colloids Surf., B 210 (2022) 112239, https://doi.org/10.1016/j.colsurfb.2021.112239.
[8] K. Ahmad, M.A. Nazi, A.K. Qureshi, E. Hussain, T. Najam, M.S. Jave, S.S.A. Shah, M.K. Tufail, S. Hussain, N.A. Khan, H.R. Shah, M. Ashfaq, Engineering of Zirconium based metal-organic frameworks (Zr-MOFs) as efficient adsorbents, Mater. Sci. Eng., B 262 (2020) 114766, https://doi.org/10.1016/j.mseb.2020.114766.
[9] M.W. Nugraha, N.H.Z. Abidin, Supandi, N.S. Sambudi, Synthesis of tungsten oxide/amino-functionalized sugarcane bagasse derived-carbon quantum dots (WO_3/N-CQDs) composites for methylene blue removal, Chemosphere 277 (2021) 130300, https://doi.org/10.1016/j.chemosphere.2021.130300.
[10] H.U.C. Serna, G.C. Domínguez, A.G. Bórquez, M.d. l.P.S. Cruz, R.R. Farrera Rebollo, Structural and luminescent properties of CQDs produced by microwave and conventional hydrothermal methods using pelagic Sargassum as carbon source, Opt. Mater. 126 (2022) 112156, https://doi.org/10.1016/j.optmat.2022.112156.
[11] M.E. Khan, A. Mohammad, T. Yoon, State-of-the-art developments in carbon quantum dots (CQDs): photo-catalysis, bio-imaging, and bio-sensing applications, Chemosphere 302 (2022) 134815, https://doi.org/10.1016/j.chemosphere.2022.134815.
[12] T.L. Tan, No A. Zulkifli, A.S.K. Zaman, M.b. Jusoh, M.N. Yaapar, S.A. Rashid, Impact of photoluminescent carbon quantum dots on photosynthesis efficiency of rice and corn crops, Plant Physiol. Biochem. 162 (2021) 737–751, https://doi.org/10.1016/j.plaphy.2021.03.031.
[13] S. Takahama, M. Kitamura, Y. Ide, K. Umemura, Variation in the responses of carbon quantum dots (CQDs) synthesized from native coconut husk and coconut husk-derived charcoal, Opt. Mater. 131 (2022) 112739, https://doi.org/10.1016/j.optmat.2022.112739.
[14] S. Kumar, J. Das, Carbon nanotubes, nanochains and quantum dots synthesized through the chemical treatment of charcoal powder, J. Mol. Struct. 1227 (2021) 129419, https://doi.org/10.1016/j.molstruc.2020.129419.
[15] D. Elango, J.S. Packialakshmi, V. Manikandan, P. Jayanthi, Synthesis of crab-shell derived CQDs for Cd2+ detection and antibacterial applications, Mater. Lett. 313 (2022) 131822, https://doi.org/10.1016/j.matlet.2022.131822.
[16] H. Xu, L. Yan, V. Nguyen, Y. Yu, Y. Xu, One-step synthesis of nitrogen-doped carbon nanodots for ratiometric pH sensing by femtosecond laser ablation method, Appl. Surf. Sci. 414 (2017) 238–243, https://doi.org/10.1016/j.apsusc.2017.04.092.
[17] J.R. Prekodravac, M.D. Budimir, D.N. Kleut, B.R. Vasiljević, V.B. Rajić, G. Ciasca, et al., Surface functionality as a key parameter for the conductivity of microwave synthesized CQDs thin films, Diam. Relat. Mater. 129 (2022) 109366, https://doi.org/10.1016/j.diamond.2022.109366.
[18] Y. Xu, W. Lu, G. Xu, T.W. Chou, Structural supercapcaitor composites: a review, Compos. Sci. Technol. 204 (2021) 108636, https://doi.org/10.1016/j.compscitech.2020.108636.
[19] Z. Zhai, J. Xu, T. Gong, B. Cao, K. Cui, L. Hou, C. Yuan, Sustainable fabrication of N-doped carbon quantum dots and their applications in fluorescent inks, Fe (III) detection and fluorescent films, Inorg. Chem. Commun. 140 (2022) 109387, https://doi.org/10.1016/j.inoche.2022.109387.
[20] K. Shireesha, V. Divya, G. Pranitha, C. Ashok, C.C. Shilpa, V. Himabindu, Asystematic investigation on the effect of reducing agents towards specific capacitance of NiMg@OH/reduced graphene oxide nanocomposites, Mater. Technol.: Adv. Perform. Mater. 37 (2022) 1864–1876, https://doi.org/10.1080/10667857.2021.1995933.
[21] C. Zhao, W. Zheng, A review for aqueous electrochemical supercapacitors, Front. Energy Res. 3 (2015) 23, https://doi.org/10.3389/fenrg.2015.00023.
[22] J.P. Reddy, J.W. Rhim, Extraction and characterization of cellulose microfibers from agricultural wastes of onion and garlic, J. Nat. Fibers 15 (2018) 465–473, https://doi.org/10.1080/15440478.2014.945227.
[23] T.L. Tan, N.A. Zulkifli, A.S.K. Zaman, M.B. Jusoh, M.N. Yaapar, S.A. Rashid, Impact of photoluminescent carbon quantum dots on photosynthesis efficiency of rice and corn crops, Plant Physiol. Biochem. 162 (2021) 737–751. https://doi:10.1016/j.plaphy.2021.03.031.
[24] G.V. Lowry, R.J. Hill, S. Harper, A.F. Rawle, C.O. Hendren, F. Klaessig, et al., Guidance to improve the scientific value of zeta-potential measurements in nanoEHS, Environ. Sci.: Nano 3 (2016) 953–965, https://doi.org/10.1039/C6EN00136J.
[25] B.T. Hoan, P.D. Tam, V.H. Pham, Green synthesis of highly luminescent carbon quantum dots from lemon juice, Journal of Nanotechnology (2019), https://doi.org/10.1155/2019/2852816. Article ID 2852816.
[26] C. Baslak, S. Demirel, A. Kocyigit, H. Alatli, M. Yildirim, Mater. Sci. Semicond. Process. 147 (2022) 106738, https://doi.org/10.1016/j.mssp.2022.106738.
[27] M.S.A. Ja'farawy, Kusimandari, A. Purwanto, H. Widiyandari, Carbon quantum dots supported zinc oxide (ZnO/CQDs) efficient photocatalyst for organic pollutant degradation–A systematic review, Environ. Nanotechnol. Monit. Manag. 18 (2022) 100681, https://doi.org/10.1016/j.enmm.2022.100681.
[28] Q. Wang, C. Zhang, G. Shen, H. Liu, H. Fu, D. Cui, Fluorescent carbon dots as an efficient siRNA nanocarrier for its interference therapy in gastric cancer cells, J. Nanobiotechnol. 12 (2014) 58, https://doi.org/10.1186/s12951-014-0058-0.
[29] V. Tucureanu, A. Matei, A.M. Avram, FTIR spectroscopy for carbon family study, Crit. Rev. Anal. Chem. 46 (2016) 502–520, https://doi.org/10.1080/10408347.2016.1157013.
[30] I.C.N.D. León, J. Johny, S.V. Rodríguez, N.G. Gómez, S.C. Bernal, I. Mendivil, S. Shaji, S.S. Guzmán, Tuning the luminescence of nitrogen-doped graphene quantum dots synthesized by pulsed laser ablation in liquid and their use as a selective photoluminescence on–off–on probe for ascorbic acid detection, Carbon 150 (2019) 455–464, https://doi.org/10.1016/j.carbon.2019.05.057.
[31] T. Pang, F. Marken, D. Zhang, D. Mattia, J. Shen, Linking macroscopic surface morphology of activated carbon fibres and electrosorption performance: an electrochemical impedance spectroscopy and capacitive deionization study, Appl. Surf. Sci. 609 (2022) 155397, https://doi.org/10.1016/j.apsusc.2022.155397.
[32] T.A. Burinaru, B. Adiaconiță, M. Avram, P. Preda, A.M. Enciu, E. Chiriac, C. Mărculescu, T. Constantin, Electrochemical impedance spectroscopy based microfluidic biosensor for the detection of circulating tumor cells, Mater. Today Commun. 32 (2022) 104016, https://doi.org/10.1016/j.mtcomm.2022.104016.

[33] C. Ma, K. Dai, H. Hou, X. Ji, L. Chen, D.G. Ivey, et al., High ion-conducting solid-state composite electrolytes with carbon quantum dot nanofillers, Adv. Sci. 5 (2018) 1700996, https://doi.org/10.1002/advs.201700996.
[34] M.N. Sakib, S. Ahmed, S.M.S.M. Rahat, S.B. Shuchi, A review of recent advances in manganese-based supercapacitors, J. Energy Storage 44 (2021) 103322, https://doi.org/10.1016/j.est.2021.103322.
[35] J.Y. Shieh, S.Y. Tsai, B.Y. Li, H.H. Yu, High-performance flexible supercapacitor based on porous array electrodes, Mater. Chem. Phys. 195 (2017) 114–122, https://doi.org/10.1016/j.matchemphys.2017.04.034.
[36] X. Zhao, J. Zhang, K. Lv, N. Kong, Y. Shao, J. Tao, Carbon nanotubes boosts the toughness and conductivity of wet-spun MXene fibers for fiber-shaped super capacitors, Carbon 200 (2022) 38–46, https://doi.org/10.1016/j.carbon.2022.08.045.
[37] N. Kumar, R.T. Ginting, J.W. Kang, Flexible, large-area, all-solid-state supercapacitors using spray deposited PEDOT: PSS/reduced-graphene oxide, Electrochim. Acta 270 (2018) 37–47, https://doi.org/10.1016/j.electacta.2018.03.069.
[38] J.Y. Shieh, C.H. Wu, S.Y. Tsai, H.H. Yu, Fabrication and characterization of a sandpaper-based flexible energy storage, Appl. Surf. Sci. 364 (2016) 21–28, https://doi.org/10.1016/j.apsusc.2015.11.152.
[39] G. Ma, J. Li, K. Sun, H. Peng, J. Mu, Z. Lei, High performance solid-state supercapacitor with PVA–KOH–$K_3[Fe(CN)_6]$ gel polymer as electrolyte and separator, J. Power Sources 256 (2014) 281–287, https://doi.org/10.1016/j.jpowsour.2014.01.062.
[40] Y. Zolfaghari, M. Ghorbani, M.S. Lashkenari, Electrochemical study on zeolitic imidazolate framework -67 modified $MnFe_2O_4$/CNT nanocomposite for supercapacitor electrode, Electrochim. Acta 380 (2021) 138234, https://doi.org/10.1016/j.electacta.2021.138234.
[41] X. Cheng, J. Pan, Y. Zhao, M. Liao, H. Peng, Gel polymer electrolytes for electrochemical energy storage, Adv. Energy Mater. 8 (2018) 1702184, https://doi.org/10.1002/aenm.201702184.
[42] S. Ishaq, M. Moussa, F. Kanwal, R. Ayub, D. Losic, One step strategy for reduced graphene oxide/cobalt-iron oxide/polypyrrole nanocomposite preparation for high performance supercapacitor electrodes, Electrochim. Acta 427 (2022) 140883, https://doi.org/10.1016/j.electacta.2022.140883.
[43] L. Yang, K. Zhuo, X. Xu, Z. Zhang, J. Wang, Anthraquinone-modified nitrogen-doped graphene aerogel for boosting energy density of supercapacitors by self-matching of capacity, Electrochim. Acta 393 (2021) 139057, https://doi.org/10.1016/j.electacta.2021.139057.
[44] J. Ma, Y. Yamamoto, C. Su, S. Badhulika, C.Y. Kong, One-pot microwave-assisted synthesis of porous reduced graphene oxide as an electrode material for high capacitance supercapacitor, Electrochim. Acta 386 (2021) 138439, https://doi.org/10.1016/j.electacta.2021.138439.
[45] C. Zhou, T. Gao, Q. Liu, Y. Wang, D. Xiao, Preparation of quinone modified graphene-based fiber electrodes and its application in flexible asymmetrical supercapacitor, Electrochim. Acta 336 (2020) 135628, https://doi.org/10.1016/j.electacta.2020.135628.
[46] M. Karakoti, S. Pandey, G. Tatrari, P.S. Dhapola, R. Jangra, S. Dhali, M. Pathak, S. Mahendia, N.G. Sahoo, A waste to energy approach for the effective conversion of solid waste plastics into graphene nanosheets using different catalysts for high performance supercapacitors: a comparative study, Mater. Adv. 3 (2022) 2146–2157, https://doi.org/10.1039/D1MA01136G.
[47] A. Davies, P. Audette, B. Farrow, F. Hassan, Z. Chen, J.Y. Choi, A. Yu, Graphene-based flexible supercapacitors: pulse-electropolymerization of polypyrrole on free-standing graphene films, J. Phys. Chem. C 115 (2011) 17612–17620, https://doi.org/10.1021/jp205568v.
[48] Q. Chang, L. Li, H. Qiao, L. Sai, Y. Zhang, W. Shi, L. Huang, Enhanced electrolyte ion penetration in microdome-like graphene with high mass loading for high-performance flexible supercapacitors, ACS Appl. Energy Mater. 2 (2019) 6790–6799, https://doi.org/10.1021/acsaem.9b01240.
[49] Y. Wu, Z. Zhang, W. Liu, Y. Zheng, J. Su, L. Li, N. Liu, Y. Gao, Facile synthesis of novel $Zn_5Mo_2O_{11}\cdot 5H_2O$ nanoflowers with excellent rate capability in supercapacitors, J. Power Sources 520 (2022) 230816, https://doi.org/10.1016/j.jpowsour.2021.230816.
[50] C. Gao, Y. Duan, Y. Liu, J. Gu, Z. Guo, P. Huo, A high energy density supercapacitor fabricated with aqueous polymer electrolyte based on soybean protein isolate grafted by polyacrylic acid, J. Power Sources 541 (2022) 231658, https://doi.org/10.1016/j.jpowsour.2022.231658.
[51] K.H. An, W.S. Kim, Y.S. Park, J.M. Moon, D.J. Bae, S.C. Lim, Y.S. Lee, Y.H. Lee, Electrochemical properties of high-power supercapacitors using single-walled carbon nanotube electrodes, Adv. Funct. Mater. 11 (2001) 387–392, https://doi.org/10.1002/1616-3028(200110)11:5<387::AID-ADFM387>3.0.CO;2-G.
[52] S. Zhao, C.Y. Wang, M.M. Chen, J. Wang, Z.Q. Shi, Potato starch-based activated carbon spheres as electrode material for electrochemical capacitor, J. Phys. Chem. Solid. 70 (2009) 1256–1260, https://doi.org/10.1016/j.jpcs.2009.07.004.
[53] Y. Zhou, Y. Xie, Enhanced electrochemical stability of carbon quantum dots-incorporated and ferrous-coordinated polypyrrole for supercapacitor, J. Solid State Electrochem. 22 (2018) 2515–2529, https://doi.org/10.1007/s10008-018-3964-5.
[54] E. Elanthamilan, S.J. Jennifer, S.F. Wang, J.P. Merlin, Effective conversion of Cassia fistula dry fruits biomass into porous activated carbon for supercapacitors Mater, Chem. Phys. 286 (2022) 126188, https://doi.org/10.1016/j.matchemphys.2022.126188.